Stimulation Strength and Focality of Electroconvulsive Therapy and Magnetic Seizure Therapy in a Realistic Head Model

Won Hee Lee, *Student Member, IEEE*, Sarah H. Lisanby, Andrew F. Laine, *Fellow, IEEE*, and Angel V. Peterchev, *Member, IEEE*

***Abstract*—This study examines the characteristics of the electric field (E-field) induced in the brain by electroconvulsive therapy (ECT) and magnetic seizure therapy (MST). The electric field induced by five ECT electrode configurations (bilateral, bifrontal, right unilateral, focal electrically administered seizure therapy, and frontomedial) as well as an MST coil configuration (circular) was computed in an anatomically realistic finite element model of the human head. We computed the maps of the electric field strength relative to an estimated neural activation threshold, and used them to evaluate the stimulation strength and focality of the various ECT and MST paradigms. The results show that the median ECT stimulation strength in the brain is 3–11 times higher than that for MST, and that the stimulated brain volume is substantially higher with ECT (47–100%) than with MST (21%). Our study provides insight into the observed reduction of cognitive side effects in MST compared to ECT, and supports arguments for lowering ECT current amplitude as a means of curbing its side effects.**

I. Introduction

ELECTROCONVULSIVE therapy (ECT) has unparalleled antidepressant efficacy in the treatment of severe major depression [1]. ECT induces a generalized seizure under anesthesia for therapeutic purposes using electric current delivered through electrodes placed on the scalp. However, cognitive side effects of ECT such as retrograde amnesia limit its clinical use [2]. Variations in ECT technique have been introduced in an attempt to improve the risk to benefit ratio of ECT by manipulating stimulation parameters including electrode placement and stimulus current parameters [3]. For instance, high dose right unilateral (RUL) ECT has a comparable efficacy to bilateral (BL) ECT with a significant decrease in amnesia [4]. Alternative approaches have included bifrontal (BF) ECT [5] and two experimental electrode configurations, focal electrically administered seizure therapy (FEAST) [6] and frontomedial (FM) ECT [7], to target prefrontal cortex while sparing certain brain regions (e.g., hippocampus) thought to be associated with adverse side effects of ECT [2]. Another alternative is magnetic seizure therapy (MST) which is a means to achieve more focal seizure induction using repetitive transcranial magnetic stimulation (rTMS) [8, 9].

Previously, using a spherical head model, we compared the suprathreshold direct stimulation strength and volume (focality) of ECT and MST configurations [10], showing that the E-field strength relative to threshold for MST is 3–6 times weaker and 10–60 times more focal compared with conventional ECT with 800 mA, 0.3 ms pulses. Spherical head models, however, are limited by the substantial simplification of the head anatomy and anisotropic tissue properties. In another study in a realistic head model, we quantified the induced E-field strength in various brain regions of interest (ROIs) by the BL, BF, RUL, and FEAST ECT electrode configurations [11]. However, that study used a truncated head model and the E-field characteristics of FM ECT and MST have not been investigated directly.

In this paper, we investigate the characteristics of the E-field induced in the brain by ECT and MST. We create an anatomically realistic finite element model of the whole head to simulate the E-field distribution induced by various ECT electrode and MST coil configurations. We determine the stimulation strength and focality relative to an estimated neural activation threshold to compare the E-field characteristics generated by ECT to those by MST. The comparison of the E-field stimulation strength and focality of various ECT and MST modalities could help the interpretation of clinical studies and may guide the improvement of ECT and MST dosing paradigms for reduced side effects.

II. Methods

A. Structural and Diffusion Tensor MRI Acquisition

One healthy human subject (male, age=34 years) participated in this study. T1-weighted structural magnetic resonance imaging (MRI) and diffusion tensor imaging (DTI) datasets of this subject, including the skull base and a portion of the neck underneath, were acquired on a 3 T Philips Achieva scanner (Philips Medical Systems, Best, Netherlands) using an 8-channel head coil. The T1-weighted MRI images were obtained with a 3D spoiled gradient recalled echo (SPGR) (TR=6.5 ms; TE=3.0 ms; 256 coronal slices; $1\times1\times1$ mm^3 voxel; FA=8º; 2 averages). The DTI data was also acquired by employing a single-shot spin-echo echo-planar imaging (EPI) sequence (TR=13510 ms; TE=70

This work was supported by NIH grant R01MH091083.

W. H. Lee is with the Department of Biomedical Engineering, Columbia University, New York, NY 10027 and with the Department of Psychiatry and Behavioral Sciences, Duke University, Durham, NC 27710, USA (e-mail: wl2324@columbia.edu).

S. H. Lisanby is with Department of Psychiatry and Behavioral Sciences, and Department of Psychology & Neuroscience, Duke University, Durham, NC 27710, USA (e-mail: sarah.lisanby@duke.edu).

A. F. Laine is with the Department of Biomedical Engineering, Columbia University, New York, NY 10027, USA (e-mail: laine@columbia.edu).

A. V. Peterchev is with Departments of Psychiatry and Behavioral Sciences, Biomedical Engineering, and Electrical and Computer Engineering, Duke University, Durham, NC 27710, USA (phone: 919-684-0383; fax: 919-681-9962; e-mail: angel.peterchev@duke.edu).

978-1-4244-7929-0/14/$26.00 ©2014 IEEE

ms; 112×112 acquisition matrix; FA=90º; 2×2×2 mm^3 voxel). The diffusion sensitizing gradients with a b-value of 1000 s/mm^2 were applied in 32 non-collinear directions. We corrected the DTI data for distortions due to eddy currents and subject motion artifacts using FSL (FMRIB Analysis Group, University of Oxford, UK).

B. Tissue Segmentation

To create a realistic volume conductor model of the whole head, the structural MRI images were segmented into several tissue regions (see Table I). We first removed non-brain regions using the skull-stripping algorithm BET tool in FSL. This initial segmentation was further corrected for accurate brain extraction using manual editing tools in the ITK-SNAP software [12]. The de-skulled MRI images were automatically segmented into partial volume images corresponding to gray matter, white matter, and cerebrospinal fluid (CSF) using an automated segmentation tool FAST in FSL. We then segmented non-brain regions into 11 different tissue regions, including skin, muscle, skull compacta, skull spongiosa, vertebrae, spinal cord, lens, eyeball, sclera, optic nerve, and sinus, using a combination of segmentation editing tools from the ITK-SNAP software [12] and an in-house segmentation algorithm based on thresholding and mathematical morphological operations [11, 13, 14].

C. ECT Electrode and MST Coil Configurations

For ECT, three conventional ECT electrode configurations (BL, BF, and RUL) [1] and two experimental configurations (FEAST and FM) [6, 7] were modeled (see Fig. 1). For BL ECT, the two electrodes were placed bilaterally at the frontotemporal positions located 2.5 cm above the midpoint of the line connecting the external canthus and tragus. For BF ECT, the electrodes were positioned bilaterally 5 cm above the outer angle of the orbit on a line parallel to the sagittal plane. For RUL ECT, one electrode was placed 2.5 cm to the right of vertex and the second electrode were placed in the homologous right frontotemporal position. For FEAST, a wide rectangular electrode (2.5 cm × 6.3 cm) was placed over the right motor strip and a small circular electrode (2 cm diameter) was placed over the right eyebrow [6]. For FM ECT, one electrode was placed medially on the forehead and the second electrode was placed in front of vertex [7].

For MST, we modeled a circular coil placed on vertex (CIRC, S/N MP39, Magstim Co, Whiteland, Wales, UK) using manufacturer's data and inductance measurements [10]. The CIRC coil consists of two parallel layers of windings connected in series, each with an inner diameter of 44 mm, outer diameter of 120 mm, and 9 turns (see Fig. 1). The coil conductors were centered above the vertex of the head model [8, 10].

D. Tissue Electrical Conductivity

All tissue regions were considered electrically isotropic except the white matter. We used electrical conductivity values given in Table I [11, 14] for the isotropic tissue compartments. To estimate the white matter conductivity tensors σ with variable anisotropy ratios, we deployed the volume normalized technique using the measured diffusion tensors D and the isotropic white matter conductivity σ_{iso} [15, 16]. The diffusion tensor in each voxel is linearly scaled so that the volume of the conductivity tensor equals that of an isotropic conductivity sphere with radius σ_{iso}

TABLE I
TISSUE ELECTRICAL CONDUCTIVITIES (S/M)

Tissue	Conductivity	Tissue	Conductivity
Skin	0.43	Lens	0.32
Muscle	0.32	Eyeball	0.5
Skull compacta	0.0063	Sclera	0.5
Skull spongiosa	0.04	Spinal cord	0.15
Cerebrospinal fluid	1.79	Vertebrae	0.012
Gray matter	0.33	Optic nerve	0.14
White matter (iso.)	0.14	Sinus	0

$$\sigma = \frac{\sigma_{iso}}{\sqrt[3]{d_1 \cdot d_2 \cdot d_3}} D \quad (1)$$

where d_i are the diffusion tensor eigenvalues.

E. Electric Field Simulation

To obtain the E-field distribution induced in the brain by the various ECT electrode and MST coil configurations, the complete 3-D head models incorporating ECT electrodes or MST coil were adaptively tessellated to construct realistic finite element models using the restricted Delaunay triangulation algorithm [17].

The methods to simulate the E-field strength induced by ECT and MST are described in detail in our previous studies [10, 11] and are summarized here. Since the current waveform frequencies in ECT and MST are relatively low (<10 kHz), the E-field solutions were obtained by deploying the quasi-static approximation using the finite element analysis software ANSYS (ANSYS Inc., Canonsburg, PA, USA). The spatial distribution of the E-field induced by each of the five ECT electrode configurations was computed at a current of 800 mA using the preconditioned conjugate gradient solver. A time-harmonic simulation with appropriate boundary conditions was performed to compute the spatial E-field distribution generated by CIRC MST at maximum output of the Magstim Theta device [10, 18].

F. Stimulation Strength and Focality Analysis

We simulated the E-field strength for current amplitude of 800 mA for BL, BF, and RUL ECT (conventional in clinical practice); 612 mA for FEAST (average current amplitude in [6]); and 500 mA for FM ECT (as used in [7]). MST was simulated for maximum current amplitude of a Magstim Theta device (as used in clinical studies) [8, 9].

We calculated the stimulation strength relative to a neural activation threshold by dividing the E-field magnitude in the brain by the E-field threshold, E/E_{th} [10, 14]. We used estimates of the E-field thresholds for ECT and MST derived in our previous study: 0.25 V/cm for ultrabrief ECT (rectangular pulse width=0.3 ms) and 0.64 V/cm for CIRC MST (cosine pulse duration=0.4 ms), respectively [10]. We quantified the

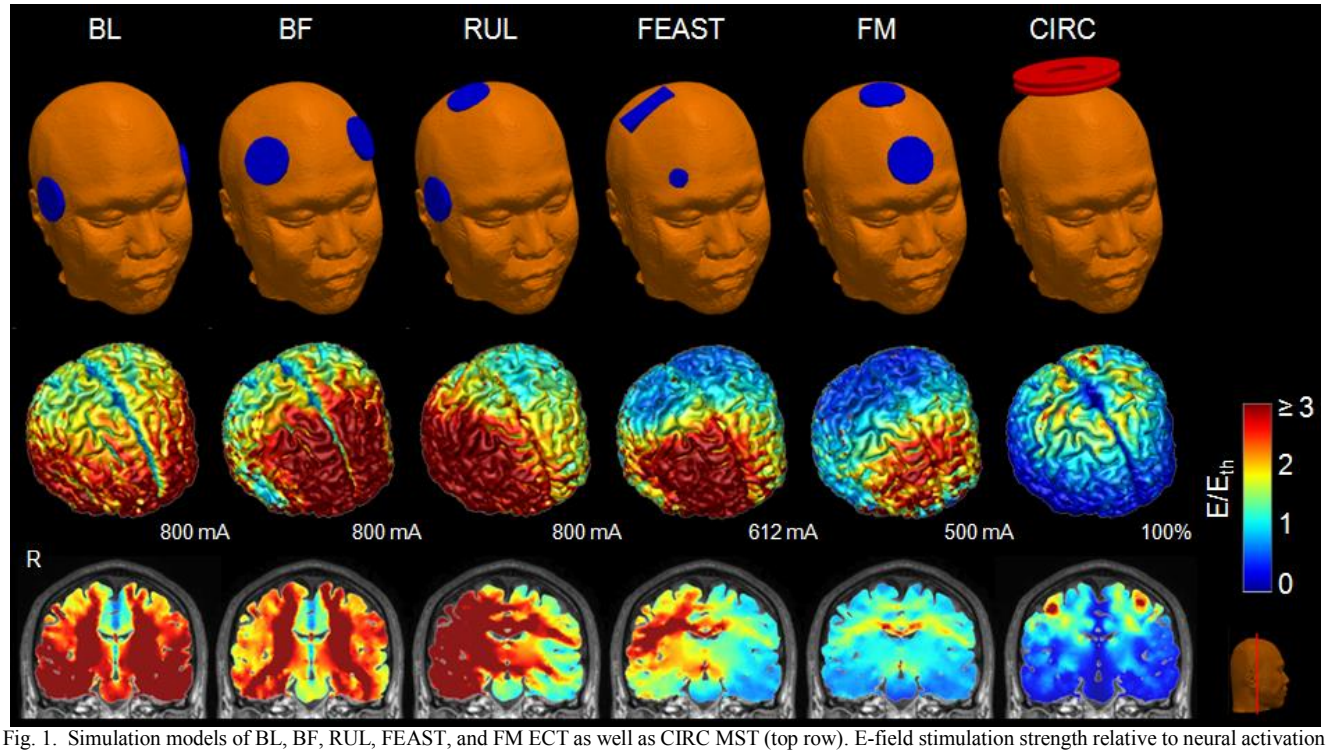

Fig. 1. Simulation models of BL, BF, RUL, FEAST, and FM ECT as well as CIRC MST (top row). E-field stimulation strength relative to neural activation threshold (E_{th}) at current of 800 mA for BL, BF, and RUL ECT, 612 mA for FEAST, 500 mA for FM ECT, and 100% Magstim Theta output for CIRC MST coil configuration on the cortical surface (middle row) and in a representative coronal slice (bottom row). E_{th} is 0.25 V/cm for ECT and 0.64 V/cm for MST. R: right.

focality of stimulation by calculating the brain volume exposed to E-field magnitude stronger than the neural activation threshold, i.e., the volume where $E/E_{th} \geq 1$ [10, 14].

III. Results

Fig. 1 shows the simulated BL, BF, RUL, FEAST, and FM ECT electrode configurations as well as the CIRC MST coil configuration, and corresponding cortical surface maps as well as coronal cross-sectional maps of the E-field distributions relative to the neural activation threshold E_{th}.

Fig. 2 (a) shows descriptive statistics on the E-field magnitude relative to the neural activation threshold for the ECT and MST modalities. The results indicate that the stimulation strength of ECT relative to the neural activation threshold is substantially higher than that of MST. The median ECT induced E-field strength ranges from 0.8 to 3.4 times threshold, corresponding to FM and BL ECT, respectively, whereas for CIRC MST it is only 0.3 times threshold (0.19 V/cm). Furthermore, the maximum E-field strength relative to threshold induced by ECT is 1.2–7.3 times higher than that by MST.

The percentage of brain volume stimulated above E-field threshold for neural activation is shown in Fig. 2(b). Among the ECT paradigms, BL at 800 mA stimulates the largest brain volume (99.8%), while FM at 500 mA produces the most focal brain stimulation (47 %). CIRC MST produces more focal stimulation (21%) than all of the ECT modalities. Thus, the stimulation by MST is 3–11 times weaker (in median value) and 2–5 times more focal than the ECT paradigms.

IV. Discussion and Conclusions

We examined the E-field stimulation strength and focality of various ECT electrode and MST coil configurations using a high-resolution, anatomically accurate, finite element model of a whole human head. The results in Fig. 1 demonstrate the different patterns of stimulation in the brain for the various ECT electrode and MST coil configurations. The substantially different E-field exposure of the brain suggests that seizure initiation and modulation by the stimulus train may have different spatial profiles across the various modalities.

Consistent with our previous findings [10], this study indicate that at the high current amplitude (800 mA) used in clinical ECT practice, the E-field in the brain exceeds the threshold for neural activation by more than 2-fold and stimulates more than 94% of the brain volume, much higher than necessary for seizure induction and possibly contributing to adverse side effects of ECT. While experimental modalities like FEAST and FM ECT produce more focal and closer to threshold stimulation by virtue of the electrode configuration and lower current amplitude, these modalities still stimulate directly more than 47% of the brain. On the other hand, CIRC MST induces the weakest, most superficial E-field, stimulating only 21% of the brain volume. Thus, MST produces very focal stimulation, that is nevertheless capable of inducing generalized seizures [8].

Taken together, these observations support exploring ECT paradigms with current amplitude lower than the minimum of conventional ECT devices (500 mA) as a means of reducing

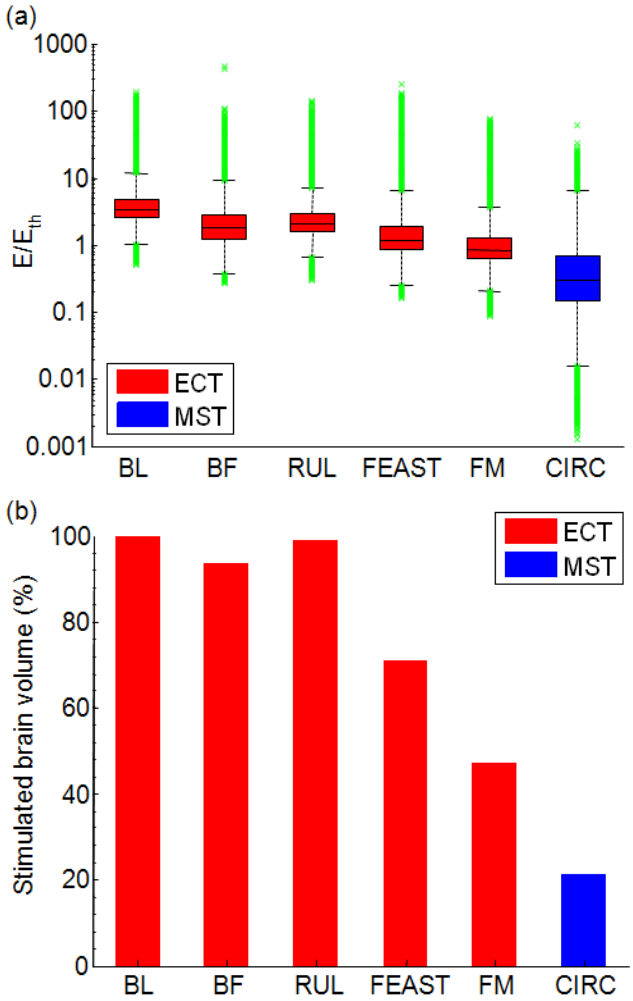

Fig. 2. (a) Descriptive statistics of E-field magnitude relative to neural activation threshold at current of 800 mA for BL, BF, and RUL ECT, 612 mA for FEAST, 500 mA for FM ECT, and 100% stimulator output for CIRC MST coil configuration. Boxes indicate the interquartile range (25th to 75th percentile) with the median marked by a horizontal black line. Whiskers delimit approximately the 99.3 percentile of the E-field distribution. Outliers beyond this range are plotted in green. (b) Percentage brain volume stimulated above neural activation threshold ($E \geq E_{th}$).

side effects. Our study further demonstrates the utility of computational E-field models to examine and compare various stimulus delivery paradigms for electric and magnetic seizure therapy, including novel electrode/coil and current amplitude configurations (e.g., FEAST and FM ECT, and CIRC MST).

V. Acknowledgement

The authors thank Dr. Zhi-De Deng for discussion of the MST modeling methods.

VI. References

[1] R. Abrams, *Electroconvulsive therapy*, 4th Ed. New York: Oxford Unversity Press, 2002.

[2] H. A. Sackeim, J. Prudic, R. Fuller, J. Keilp, P. W. Lavori, and M. Olfson, "The cognitive effects of electroconvulsive therapy in community settings," *Neuropsychopharmacology,* vol. 32, pp. 244-254, 2007.

[3] A. V. Peterchev, M. A. Rosa, Z. D. Deng, J. Prudic, and S. H. Lisanby, "Electroconvulsive therapy stimulus parameters: rethinking dosage," *J. ECT,* vol. 26, pp. 159-174, 2010.

[4] H. A. Sackeim, J. Prudic, D. P. Devanand, M. S. Nobler, S. H. Lisanby, S. Peyser, L. Fitzsimons, B. J. Moody, and J. Clark, "A prospective, randomized, double-blind comparison of bilateral and right unilateral electroconvulsive therapy at different stimulus intensities," *Arch. Gen. Psychiatry*, vol. 57, pp. 425-434, 2000.

[5] H. A. Sackeim, "Convulsant and anticonvulsant properties of electroconvulsive therapy: towards a focal form of brain stimulation," *Clin. Neurosci. Res.*, vol. 4, no.1, pp. 39-57, 2004.

[6] Z. Nahas, B. Short, C. Burns, M. Archer, M. Schmidt, J. Prudic, *et al.*, "A feasibility study of a new method for electrically producing seizures in man: focal electrically administered seizure therapy [FEAST]," *Brain Stimul,* vol. 6, pp. 403-8, 2013.

[7] M. A. Rosa, G. L. Abdo, M. O. Rosa, S. H. Lisanby, and A. V. Peterchev, "Fronto-medial electrode placement with low current amplitude: a case report," *J ECT,* vol. 28, p. 146, 2012.

[8] S. H. Lisanby, B. Luber, T. E. Schlaepfer, and H. A. Sackeim, "Safety and feasibility of magnetic seizure therapy (MST) in major depression: randomized within-subject comparison with electroconvulsive therapy," *Neuropsychopharmacology,* vol. 28, pp. 1852-1865, 2003.

[9] S. B. Rowny, K. Benzl, and S. H. Lisanby, "Translational development strategy for magnetic seizure therapy," *Exp. Neurology,* vol. 219, PP. 27-35, 2009.

[10] Z. D. Deng, S. H. Lisanby, and A. V. Peterchev, "Electric field strength and focality in electroconvulsive therapy and magnetic seizure therapy: a finite element simulation study," *J. Neural Eng.,* vol. 8, 2011.

[11] W. H. Lee, Z. D. Deng, T. S. Kim, A. F. Laine, S. H. Lisanby, and A. V. Peterchev, "Regional electric field induced by electroconvulsive therapy in a realistic finite element head model: influence of white matter anisotropic conductivity," *NeuroImage,* vol. 59, pp. 2110-2123, 2012.

[12] P. A. Yushkevich, J. Piven, H. C. Hazlett, R. G. Smith, S. Ho, J. C. Gee, and G. Gerig, "User-guided 3D active contour segmentation of anatomical structures: significantly improved efficiency and reliability," *NeuroImage,* vol. 31, pp. 1116-1128, 2006.

[13] W. H. Lee, T. S. Kim, M. H. Cho, Y. B. Ahn, and S. Y. Lee, "Methods and evaluations of MRI content-adaptive finite element mesh generation for bioelectromagnetic problems," *Phys. Med. Biol.,* vol. 51, pp. 6173-6186, 2006.

[14] W. H. Lee, S. H. Lisanby, A. F. Laine, and A. V. Peterchev, "Electric field characteristics of electroconvulsive therapy with individualized current amplitude: a preclinical study," *Conf. Proc. IEEE Eng. Med. Biol. Soc., pp. 3082-3085,* 2013.

[15] D. S. Tuch, V. J. Wedeen, A. M. Dale, J. S. George, and J. W. Belliveau, "Conductivity tensor mapping of the human brain using diffusion tensor MRI," *Proc. Natl. Acad. Sci.,* vol. 98, pp. 11697-11701, 2001.

[16] H. Hallez, S. Staelens, and I. Lemahieu, "Dipole estimation errors due to not incorporating anisotropic conductivities in realistic head models for EEG source analysis," *Phys. Med. Biol.,* vol. 54, pp. 6079-6093, 2009.

[17] J. P. Pons, E. Segonne, J. D. Boissonnat, L. Rineau, M. Yvinec, and R. Keriven, "High-quality consistent meshing of multi-label datasets," *Inf. Process. Med. Imaging,* vol. 20, pp. 198-210, 2007.

[18] Z. D. Deng, S. H. Lisanby, and A. V. Peterchev, "Electirc field depth-focality tradeoff in transcranial magnetic stimulation: simulation comparison of 50 coil designs," *Brain Stimulation,* vol. 6, pp. 1-13, 2013.